# Equation of State of Acetic Acid Derived by Molecular-Dynamics Simulations on a Rigid-Molecule Model

**Yosuke Kataoka*** **and Mitsuhiro Matsumoto†**

Department of Materials Chemistry, College of Engineering, Hosei University, 3-7-2 Kajino-cho, Koganei, Tokyo 184

†Department of Applied Physics, School of Engineering, Nagoya University, Furo-cho, Chikusa-ku, Nagoya 464-01

(Received February 26, 1997)

The equation of state of an acetic acid fluid was derived by molecular-dynamics simulations on a rigid-molecule model. The optimized potential for liquid simulations (OPLS) given by Briggs, Nguyen, and Jorgensen was assumed. Only the *Z* form was adopted in the two conformers in order to save central processing unit (CPU) time to perform the molecular-dynamics simulation at many state points. Microcanonical simulations were performed for 729 states. The system had 256 molecules in the cubic basic cell. The equation of state was obtained by a least-squares fitting. The critical point and liquid-vapor phase boundary were compared with the observed values. Dimerization was also observed by 27 long runs in the gaseous phase around the liquid–vapor phase boundary. The main structure is hydrogen-bonded chains in the liquid phase. The excess entropy after subtracting the ideal gas term is $-10R$ at low temperatures. This is compared with $-8R$ in liquid water. These comparisons show that the present model can be used to simulate the hydrogen-bonded fluid of acetic acid.

Molecular-dynamics simulations are expected to be one of the most powerful methods to investigate the molecular mechanism of vaporization and condensation.[1,2] A hydrogen-bonded system is frequently compared with a simple fluid. Among them, acetic acid is interesting because of the stable dimer in its gaseous phase at low temperatures. Its vaporization process has been studied using a molecular beam.[3] We plan to examine such process by a molecular-dynamics (MD) simulation in a following paper.

A realistic and, at the same time, simple model should be used in any time-consuming molecular-dynamics study on such processes. In the case of water and methanol, rigid molecule models are useful for simulating the static[4—6] and dynamic[1,2] properties of the liquid–vapor interface. This paper is a report which shows the effectiveness of a simple rigid model on the acetic acid molecule. The optimized potentials for liquid simulations (OPLS) given by Briggs et al.[7] were assumed in order to obtain the equation of state of acetic acid in the liquid and the gaseous phase by a molecular-dynamics simulation.[8] They have already shown that this can give a realistic liquid state under ambient pressure based on a Monte-Carlo (MC) simulation. In their study, the molecule had a torsion degree of freedom. They showed that the *Z*-form of the two conformers is the main component, with the concentration being more than 97%. For this reason, only the *Z*-form is adopted here.

In the second section, both the model and method of the simulation are given. Then, the radial distribution functions based on MD are compared with those based on the Monte-Carlo results.[7] It will be shown that the liquid structure based on the present rigid model coincides with that based on the flexible model by MC.[7]

Microcanonical molecular-dynamics simulations were performed for 729 states. The system consisted of 256 molecules in the cubic basic cell. The equation of state was obtained by a least-squares fitting in a way similar to that of Ree.[9] The critical points and liquid–vapor phase boundary were compared with the experimentally observed values. Dimerization was also observed.

In the last section, the thermodynamic properties are surveyed as functions of the temperature at constant pressure. The entropy is compared with that in water and a Lennard–Jones liquid in order to discuss the ordering in acetic acid.

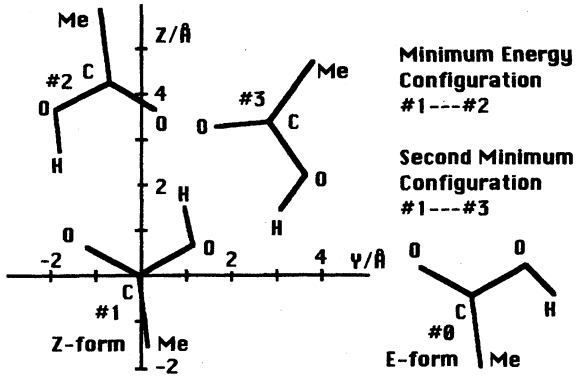


Fig. 1. The standard orientation of the *Z*-form acetic acid molecule (#1) and that of the *E*-form (#0). The #1—#2 pair shows the minimum energy configuration. The second minimum one is described as the #1—#3 pair.

## Model and Molecular-Dynamics Simulation

**Model.** Molecules are represented by interaction sites located on each nucleus, with the exception that a united model is used for methyl groups that have a single site centered on the carbon. There are two conformers in an acetic acid molecule, i.e., the *E*-form and the *Z*-form (Fig. 1). Briggs et al. studied liquid acetic acid based on an MC simulation with OPLS and a torsion potential function.[7] They showed that the *Z*-form is the main component (more than 97%). We assumed a rigid model of only the *Z*-form for simplicity in heavy simulations to obtain the equation of state. The standard orientation of the *Z*-form is shown as #1 in Fig. 1. The intermolecular potential $\phi$ is written as

$$\phi = \sum_{ij} \left\{ \frac{q_i q_j e^2}{4\pi\varepsilon_0 r_{ij}} + \frac{A_{ij}}{r_{ij}^{12}} - \frac{C_{ij}}{r_{ij}^{6}} \right\},$$

$$A_{ii} = 4\varepsilon_i \sigma_i^{12}, \quad C_{ii} = 4\varepsilon_i \sigma_i^{6}, \tag{1}$$

$$A_{ij} = \sqrt{A_{ii}A_{jj}}, \quad C_{ij} = \sqrt{C_{ii}C_{jj}}.$$

Here, the first part is the Coulomb energy, where $e$ is the elementary charge and $\varepsilon_0$ is the dielectric constant of a vacuum; the rest is the Lennard–Jones (LJ) interaction. The symbols $q_i$, $A_{ii}$, $B_{ii}$, $\varepsilon_i$, and $\sigma_i$ are the potential constants. The values of $q_i$, $\varepsilon_i$, and $\sigma_i$ are given in Table 1.[7] The pair of the #1 and #2 molecule in Fig. 1 demonstrates the configuration corresponding to the minimum pair energy. This is a cyclic dimer due to the two hydrogen bonds. The other pair, #1—#3, images the second lowest energy configuration. There are also two hydrogen bonds in this case.

Figure 2 describes the pair energy of the #1 and #2 configuration as a function of the intermolecular distance between the center of mass ($r$), where the orientations are those shown in Fig. 1. The orientational dependencies of the pair energy are shown in Fig. 3, where the orientation of the #1 molecule is fixed as in Fig. 1. The axis of rotation of the #2 molecule is the $x$-axis. Figure 2 shows that the minimum-energy configuration is realized around the point where the repulsive part of the LJ part becomes effective when the molecular distance ($r$) is decreased. We can see that the main part of the well depth of the minimum energy is the Coulomb interaction part in Figs. 2 and 3. The anisotropy is sharp in Fig. 3. This is not so sharp in the water case.[10]

**Molecular-Dynamics Simulation at Normal Density.** Molecular-dynamics calculations were carried out for a microcanonical ensemble, where the number of molecules ($N$), the volume ($V$), and the total energy ($E$) were constant. The program calculated the temporal evolution of the system using a leapfrog algorithm.[8] The electrostatic forces and energy were calculated by the Ewald's method.[8] A periodic boundary condition was assumed on the cubic cell. The force was cut off at half the MD cell width for the 256-molecule system. In the first place, some molecular-dynamics simulations were performed in order to see wheter the present rigid model can reproduce the liquid acetic acid at normal density. The starting configuration was a distorted face-centered cubic (FCC) lattice. Liquid samples were obtained by the simulated annealing method.

Figure 4 shows the radial distribution function for a carbonyl–oxygen–hydrogen pair at 300 K. The case of hydroxy–oxygen–hydrogen pair is described in Fig. 5. The height of the first peak is in agreement within 5% error with that on the flexible model by Briggs et al.[7] This result is reasonable because of the low concentration (2—3%) of the

Table 1. OPLS Potential Parameters for Acetic Acid[7]

| | $q$/e | $\sigma/10^{-10}$ m | $\varepsilon$/kcal mol$^{-1}$ |
|---|---|---|---|
| O | −0.58 | 3.00 | 0.170 |
| C | 0.55 | 3.75 | 0.105 |
| =O | −0.50 | 2.96 | 0.210 |
| H | 0.45 | 0.00 | 0.000 |
| $CH_3$ | 0.08 | 3.71 | 0.160 |

1 kcal mol$^{-}$ = 4.184 kJ mol$^{-1}$.

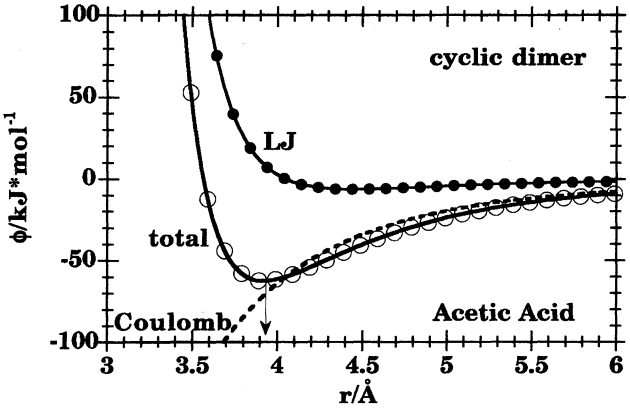


Fig. 2. The pair energy $\phi$ as a function of the intermolecular distance $r$. The orientation of the pair is fixed at the minimum energy configuration shown as #1 and #2 in Fig. 1. The contribution of the LJ part and that of Coulomb term are also shown. The arrow indicates the minimum.

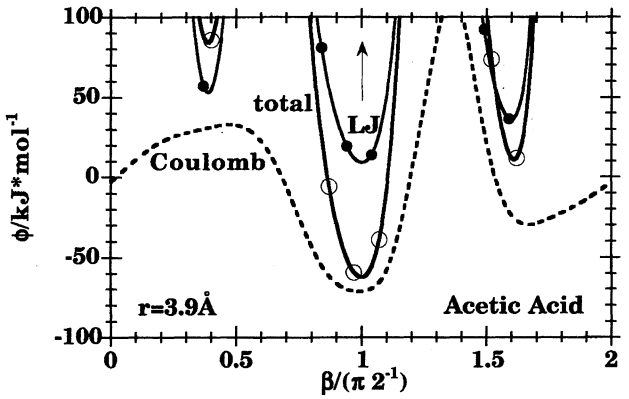


Fig. 3. The pair energy $\phi$ as a function of the orientation of the second molecule. The orientation of the first one is fixed at the standard orientation (#1 in Fig. 1). The molecular distance is that of the minimum energy configuration. The axis of rotation of the #2 molecule is the molecule-fixed $x$-axis and the rotation angle is $\beta$.

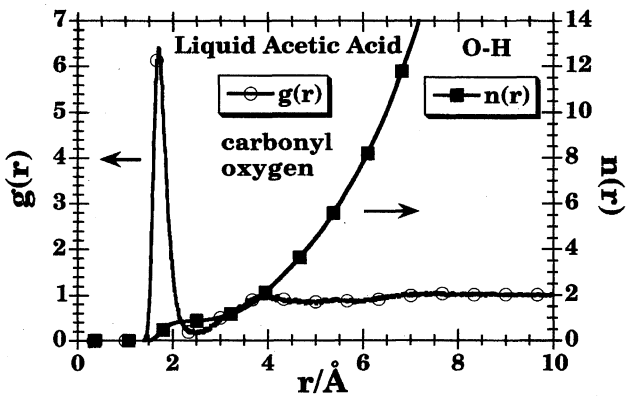


Fig. 4. The radial distribution function $g(r)$ of the cabonyl–oxygen–hydrogen pair at 300 K, $V/N$=100 Å$^3$. The running coordination number $n(r)$ is read by the axis in the right hand side.

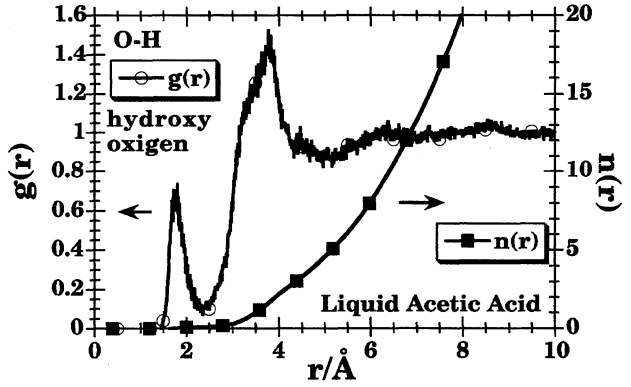


Fig. 5. The radial distribution function $g(r)$ of the hydroxy–oxygen–hydrogen pair at 300 K, $V/N$=100 Å$^3$. The axis of running coordination number $n(r)$ is shown in the right hand side.

minor component (E) in their calculation. It is clearly seen that there is one hydrogen bond in carbonyl–oxygen–hydrogen pair. Only a negligible bond is seen in the hydroxy–oxygen–hydrogen pair. Therefore, liquid acetic acid consists mainly of hydrogen-bonded chains, as shown by Briggs et al.[7] The thermodynamic properties are compared for the two models later (Table 4).

**Molecular-Dynamics Simulation for the Equation of State.** High-temperature samples at several densities were cooled in order to obtain data at many temperatures. The simulated states are shown in Fig. 6. The time step is $0.75\times10^{-15}$ s in the liquid and intermediate density and $1\times10^{-15}$ s in the gaseous state. In our standard runs, 5000 steps were used to control the temperature and aging of the system. After this, a 5000-step run was performed, where the molecular-dynamics statistical averages were obtained. Some very high-temperature data were obtained to make the fitting of the equation of state stable. Moreover, 30 states were also added around the critical points.

In the gaseous phase, it took a very long time to establish the equilibrium state at low temperatures, because of dimerization. An extreme case is shown in Fig. 7, where several physical properties are plotted against time in the case of low

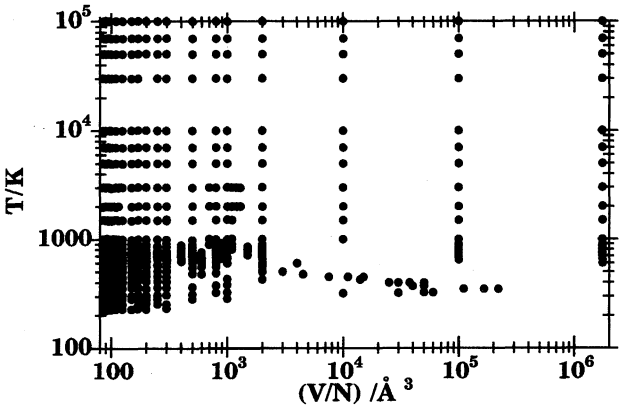


Fig. 6. The map of the simulated states in the ($V/N$, $T$) plane.

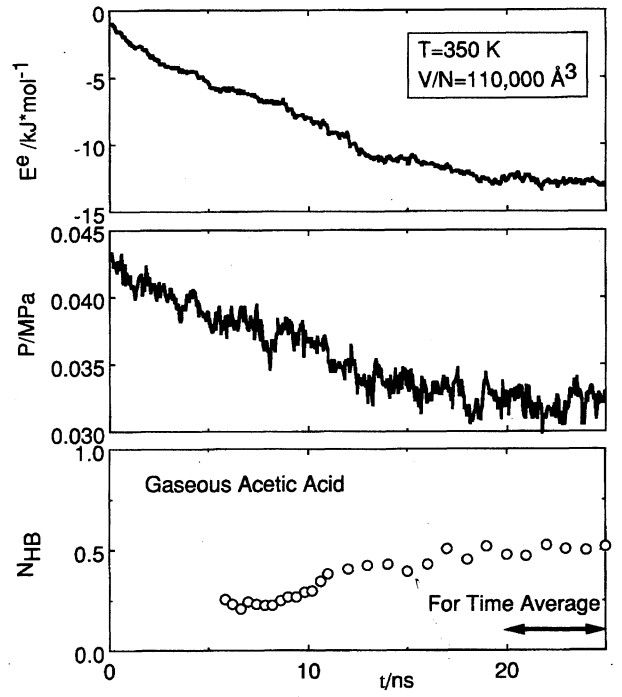


Fig. 7. An example of time development of physical properties during a MD simulation. The potential energy of the system $E^e$, the pressure $P$ and the number of hydrogen-bonded pair per molecule $N_{HB}$ are shown as a function of time $t$.

temperature (350 K) and low density (volume per molecules $V/N$ is $1.1\times10^5$ Å$^3$). Due to the slow dimerization process, the relaxation is extremely slow; we had to equilibrate the system for as long as 20 ns before taking the time average. The final configuration is shown in Fig. 8, where several cyclic dimer pairs and a trimer pair can be clearly observed. This dimerization is quantitatively analyzed in a later section. Full listings of all volumes ($V$), temperatures ($T$), energies ($E$), and pressures ($P$) are available from the authors upon request.

## Equation of State

Ree's method[9] is used to obtain the equation of state of fluid. The density is written as $\rho$ (=$N/V$) and $\beta=1/kT$. The

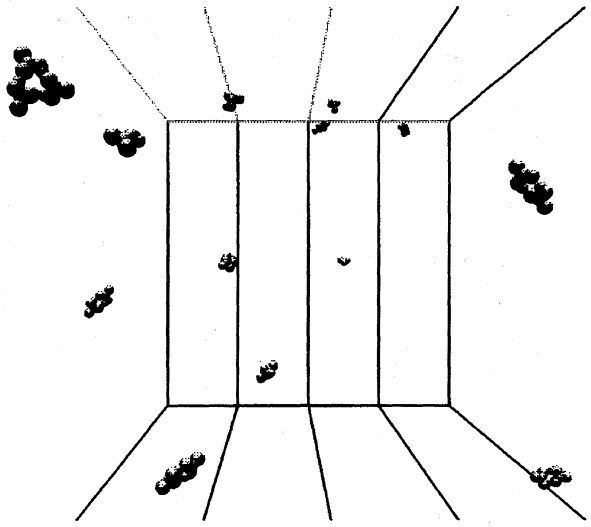

Fig. 8. A snapshot of acetic acid gas. The condition is the same as in Fig. 7, only a part of the whole system is shown.

excess Helmholtz free energy ($A^e$) (after subtracting the ideal gas term) is given as

$$\frac{\beta A^e}{N} = \int_0^\rho \left(\frac{\beta P}{\rho} - 1\right)\frac{1}{\rho}d\rho, \tag{2}$$

where the excess internal energy ($E^e$) is given by

$$E^e = \left(\frac{\partial \beta A^e}{\partial \beta}\right)_\rho. \tag{3}$$

When the pressure is given as a function of the temperature and density, as usual,[11] a numerical derivation of the other thermodynamic quantities is not simple. On the other hand, it is easy to obtain the thermodynamic quantities from the Helmholtz free energy. For this reason, we assume the following analytic expression for the excess Helmholtz free energy:[9]

$$\frac{\beta A^e}{N} = \sum_p \sum_q A_{pq}\rho_r^p \beta_r^q, \tag{4}$$

$$\begin{aligned} &p = 0, 1, 2, 3, 4, 5, 6, 7, \\ &q = 0, 1, 2, 3, 4, 5, 6, 7, \\ &p = q = 0, \text{ and } p = q = 7 \text{ are excluded,} \end{aligned} \tag{5}$$

$$\rho_r = \frac{\rho}{\rho_0}, \quad \beta_r = \frac{\beta}{\beta_0}, \tag{6}$$

$$\rho_0 = \frac{N}{V_0}, \quad \beta_0 = \frac{1}{\varepsilon_0}, \tag{7}$$

$$\frac{V_0}{N} = 300 \times 10^{-30} m^3, \quad \frac{\varepsilon_0}{k} = 3000 K. \tag{8}$$

The expansion (4) is a type of high-temperature expansion. The expansion (4) is also a density expansion. The expansion is performed by means of the dimensionless reduced quantities as Eq. 6.

The coefficients ($A_{pq}$) are obtained by a least-squares fitting. The following quantity was minimized in our case:

$$\sum_i^L \left[\left\{\frac{E_i^e}{N\varepsilon_0}\beta_r - \sum_p\sum_q qA_{pq}\rho_{ir}^p\beta_{ir}^q\right\}^2 + \left\{\left(\frac{\beta_i P_i}{\rho_i} - 1\right) - \sum_p\sum_q pA_{pq}\rho_{ir}^p\beta_{ir}^q\right\}^2\right], \tag{9}$$

$$\rho_{ir} = \frac{\rho_i}{\rho_0}, \quad \beta_{ir} = \frac{\beta_i}{\beta_0}, \tag{10}$$

$$L = 729. \tag{11}$$

The number of coefficients ($A_{pq}$) was 62. This can be compared with the simple case of Lennard–Jones fluids where 32 coefficients are used.[11] The total number of data points (729) was large enough to determine 62 coefficients in our complex fluid. The coefficients ($A_{pq}$) are given in Table 2.

The relative deviation was obtained as follows:

$$\frac{\left\langle\left[\delta\left(\frac{E^e}{N\varepsilon_0}\beta_r\right)\right]^2 + \left[\delta\left\{\frac{PV}{NkT} - 1\right\}\right]^2\right\rangle^{\frac{1}{2}}}{\left\langle\left(\frac{E^e}{N\varepsilon_0}\beta_r\right)^2 + \left\{\frac{PV}{NkT} - 1\right\}^2\right\rangle^{\frac{1}{2}}} = 0.036. \tag{12}$$

The contributions from the energy and pressure are shown below:

$$\frac{\left\langle\left[\delta\left(\frac{E^e}{N\varepsilon_0}\beta_r\right)\right]^2\right\rangle^{\frac{1}{2}}}{\left\langle\left(\frac{E^e}{N\varepsilon_0}\beta_r\right)^2\right\rangle^{\frac{1}{2}}} = 0.029, \tag{13}$$

$$\frac{\left\langle\left[\delta\left\{\frac{PV}{NkT} - 1\right\}\right]^2\right\rangle^{\frac{1}{2}}}{\left\langle\left\{\frac{PV}{NkT} - 1\right\}^2\right\rangle^{\frac{1}{2}}} = 0.072. \tag{14}$$

Figures 9, 10, and 11 show how the least-square fitting smoothes the data. The solid curve is the equation of state (EOS). The circles and triangles are the MD results. It can be seen that the temperature dependence of the pressure and excess internal energy at a given volume is well reproduced. Note that the least-square fitting was performed in a reduced variable space, as shown in Fig. 9. Figure 10 shows an example of the low-temperature data. Note that the potential energy ($E^e$), is not close to zero, even at a very low density at 400 K because of dimerization. The $P$–$V$ curve in Fig. 11 corresponds to that around the critical temperature determined by the MD-EOS. The near-critical and supercritical behavior of the fluid are observed by a much larger system. The present critical temperature is overestimated because of the small system size ($N$=256).

## Comparison of the $P$–$V$–$T$ Relation with Experiments

The critical point is determined by the condition as the common zero point of the first and second derivatives of the $P$ versus $V$ curve for a given temperature. The critical constants are compared with the observed ones[12] in Table 3. Although the calculated critical pressure is larger than the

Table 2. Coefficients $A_{pq}$

| $p$ | $q$ | $A_{pq}$ | $p$ | $q$ | $A_{pq}$ | $p$ | $q$ | $A_{pq}$ |
|---|---|---|---|---|---|---|---|---|
| 0 | 1 | 5.1690590E−02 | 2 | 6 | 6.8669138E−04 | 5 | 3 | 5.2783530E−02 |
| 0 | 2 | −5.3146366E−02 | 2 | 7 | −1.6100705E−05 | 5 | 4 | −1.6270881E−03 |
| 0 | 3 | 1.4776003E−02 | 3 | 0 | −6.0463279E−01 | 5 | 5 | −5.4357667E−04 |
| 0 | 4 | 3.2616992E−04 | 3 | 1 | 1.7515063E+00 | 5 | 6 | 4.2673386E−05 |
| 0 | 5 | −5.7763961E−04 | 3 | 2 | −9.9322057E−01 | 5 | 7 | −7.8939172E−07 |
| 0 | 6 | 6.1543993E−05 | 3 | 3 | 2.3787189E−01 | 6 | 0 | 2.5440779E−02 |
| 0 | 7 | −1.8689568E−06 | 3 | 4 | −2.2684960E−02 | 6 | 1 | −9.2017628E−02 |
| 1 | 0 | 8.0984049E−02 | 3 | 5 | 4.2996972E−04 | 6 | 2 | 5.8153812E−02 |
| 1 | 1 | 1.4208907E+00 | 3 | 6 | −1.6128826E−05 | 6 | 3 | −1.3638753E−02 |
| 1 | 2 | −1.5171448E+00 | 3 | 7 | 1.6160285E−06 | 6 | 4 | 1.0649711E−03 |
| 1 | 3 | 6.3279426E−01 | 4 | 0 | 3.9253604E−01 | 6 | 5 | 2.3067183E−05 |
| 1 | 4 | −1.3833128E−01 | 4 | 1 | −1.1628509E+00 | 6 | 6 | −4.1780700E−06 |
| 1 | 5 | 1.5456029E−02 | 4 | 2 | 6.0900807E−01 | 6 | 7 | 7.7054395E−08 |
| 1 | 6 | −8.7077270E−04 | 4 | 3 | −1.0576335E−01 | 7 | 0 | −1.8520622E−03 |
| 1 | 7 | 1.9315099E−05 | 4 | 4 | −1.6596013E−03 | 7 | 1 | 7.2463760E−03 |
| 2 | 0 | 6.1338300E−01 | 4 | 5 | 1.9735561E−03 | 7 | 2 | −4.9286508E−03 |
| 2 | 1 | −1.8468776E+00 | 4 | 6 | −1.3155783E−04 | 7 | 3 | 1.2813018E−03 |
| 2 | 2 | 1.4948777E+00 | 4 | 7 | 2.2551269E−06 | 7 | 4 | −1.3479266E−04 |
| 2 | 3 | −5.7959110E−01 | 5 | 0 | −1.3972141E−01 | 7 | 5 | 4.1784278E−06 |
| 2 | 4 | 1.1589380E−01 | 5 | 1 | 4.6041313E−01 | 7 | 6 | 1.4775729E−08 |
| 2 | 5 | −1.2064481E−02 | 5 | 2 | −2.6366338E−01 | | | |

E-02 means $10^{-2}$.

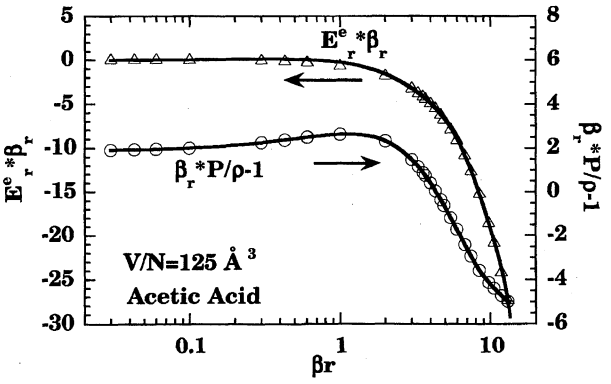


Fig. 9. Examples of fitting of the reduced excess internal energy $E^e$ multiplied by the inverse of the temperature $\beta_r$ and the compressibility factor minus one as a function of the inverse of the reduced temperature $\beta_r$ at a constant volume $V$. A liquid-like state $V/N$=125 Å$^3$ is shown.

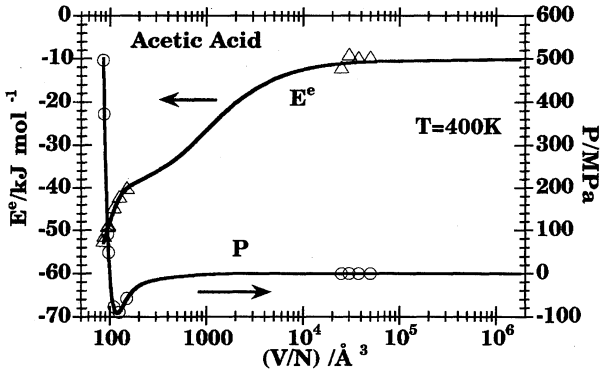


Fig. 10. An example of fitting of the excess internal energy $E^e$ and the pressure $P$ as a function of volume per molecule $V/N$ at a constant temperature $T$. The low temperature state $T$=400 K.

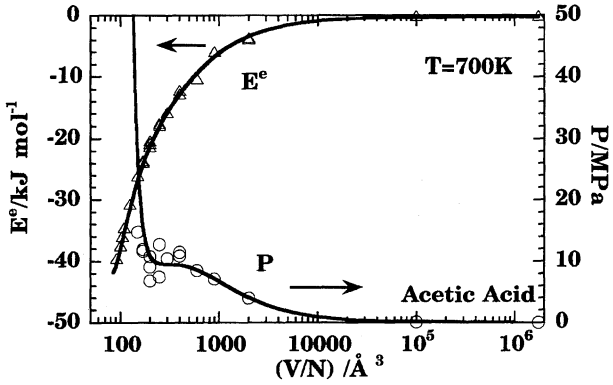


Fig. 11. An example of fitting of the excess internal energy $E^e$ and the pressure $P$ as a function of volume per molecule $V/N$ at $T$=700 K, around the critical temperature.

Table 3. Liquid–Gas Critical Constants of Acetic Acid

| | Calcd | Obsd[12] | Calcd/Obsd |
|---|---|---|---|
| $T_c$/K | 699 | 594.45 | 1.18 |
| $V_c$/cm$^3$ mol$^{-1}$ | 185 | 171 | 1.08 |
| $P_c$/MPa | 9.39 | 5.79 | 1.62 |
| $P_cV_c/NkT_c$ | 0.300 | 0.200 | 1.50 |

experimental values, the other quantities are in accordance with the observed ones. In the following, all state properties are reduced with the critical quantities in a comparison with the experimental values.

The liquid–gas phase boundary is shown in Fig. 12. It was obtained using Maxwell's rule. It can be seen that the phase boundary is in good agreement with the experiments[12] if it is reduced with the critical quantities. The $P$–$V$–$T$ relation is plotted in Fig. 13 at several temperatures. An empiri-

Table 4. Comparison with the Monte Carlo and Observed Results under Normal Pressure[a)]

| $T$/K | 298 | | | 373 | | |
|---|---|---|---|---|---|---|
| Method | EOS | MC[7)] | Obsd[15–18)] | EOS | MC[7)] | Obsd[15–18)] |
| $(V/N)$/Å$^3$ | 91.9 | 95.8 | 95.5 | 97.1 | 102.6 | 104.1 |
| $E^e$/kJ mol$^{-1}$ | −54.4 | −51.92 | −52.26[b)] | −50.1 | −47.32 | −47.28[b)] |
| $\alpha$/(10$^{-3}$ K$^{-1}$) | 0.64 | 0.77 | 1.083 | 0.86 | 0.88 | 1.234 |
| $k_T$/(10$^{-9}$ Pa$^{-1}$) | 0.42 | 0.60 | | 0.60 | 0.80 | |
| $C_p^e$/kJ mol$^{-1}$ | 48 | 42.5 | 57.8 | 67 | 54.2 | 62.8 |

a) $P$=0.1 MPa. b) Estimated from heat of vaporization to ideal gas.

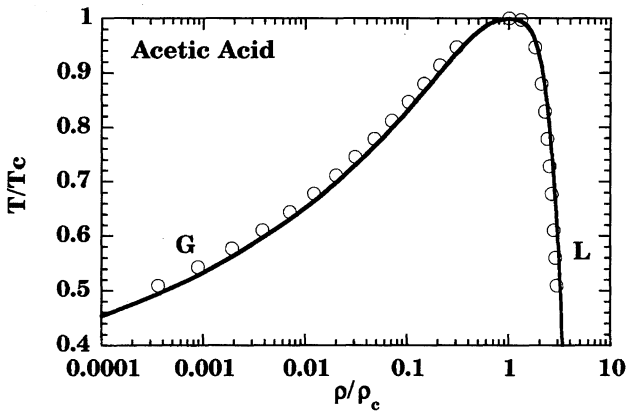


Fig. 12. The liquid–gas phase boundary is shown in the ($\rho/\rho_c$, $T/T_c$) plane. The solid curve is EOS and the circles are the observed results.[12)]

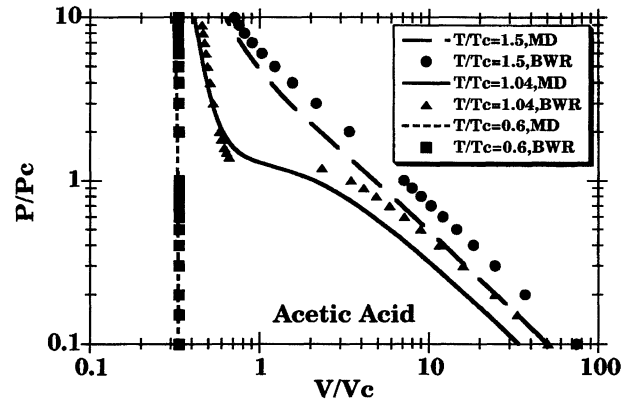


Fig. 13. The reduced pressure $P/P_c$ vs. the reduced volume $V/V_c$ plot at several temperatures obtained by MD-EOS is compared with that by BWR-EOS.[13)]

cal Benedict Webb Rubin (BWR) EOS[13)] is also shown for a comparison, because the experimental $P$–$V$–$T$ data were available to the authors at only around the saturated pressure. The lines are the MD-based EOS. The overall coincidence is given in Fig. 13.

The volume ($V$) of a liquid under ambient pressure is plotted against the temperature in Fig. 14. The thermal-expansion coefficient ($\alpha$) is also shown here. We can see that the present EOS gives a reasonable volume when compared with the observed one[12)] in reduced space.

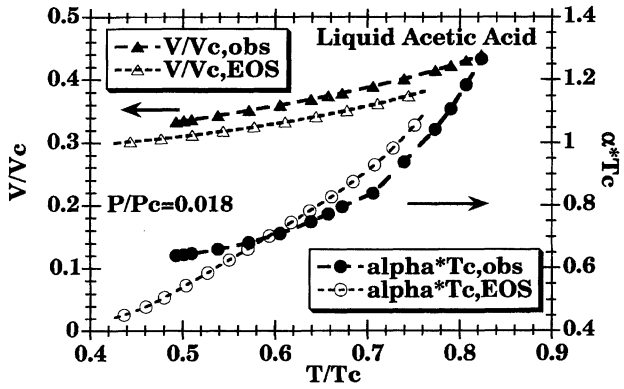


Fig. 14. The reduced volume $V/V_c$ (the left hand axis) vs. the reduced temperature $T/T_c$ plot is compared with the observed values[15)] under the ambient pressure $P/P_c$=0.0175 in the liquid phase. The thermal expansion coefficient is also compared by the right hand axis.

## Dimerization in the Gaseous Phase

Figure 15 depicts the compressibility factor, $Z=PV/NkT$, as a function of the density at low temperatures. The low-density limit is also shown as only a guide for the eye. It is compared with Bich et al.'s experimental data.[14)] It is well known that this has a value that is very close to unity in a normal gas. The calculated value is clearly less than that

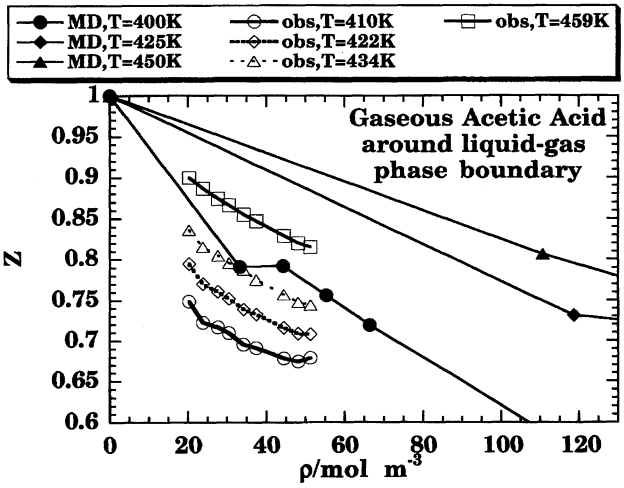


Fig. 15. The compressibility factor $Z=PV/NkT$ versus density $\rho$ plot around the gaseous phase branch in the liquid–gas phase boundary. The low density limit and lines are only for a guide of eye. The experimental results are also plotted.[14)]

in such a low-density region. Although the agreement is not very good, the MD data show the effect of dimerization. Dimerization is also seen in the potential energy in Fig. 10. The minimum pair energy is $-60\,\mathrm{kJ\,mol^{-1}}$. This means that the potential energy of the system ($-30\,\mathrm{kJ\,mol^{-1}}$) is the case of the minimum-energy configuration. The observed value of the potential energy ($E^e=-10\,\mathrm{kJ\,mol^{-1}}$) at 400 K shows dimerization to a large extent.

An analysis of hydrogen bonds in the gaseous acetic acid was performed as follows. Any pair of molecules is classified to be bonded if it satisfies the conditions on the atomic distance and the pair energy:

$$\begin{aligned} &r\mathrm{OH} \leq 2.5\ \text{Å}, \qquad \text{O is carbonyl oxgen,} \\ &\phi \leq -16.7\,\mathrm{kJ\,mol^{-1}}. \end{aligned} \tag{15}$$

A pair with two bonds is called a cyclic dimer. A non-cyclic dimer has only one bond. The mole fractions of these and the monomer were obtained as in Fig. 16. The states are near to the phase boundary. It can be seen that about 50% is the dimer at low temperatures. The mole fraction of the monomer increases as a function of the temperature as a general trend. The equilibrium constant in the chemical reaction was calculated. The result is shown in Fig. 17. The order of magnitude of the equilibrium constant of dimerization is in an agreement with the experimental value of around 400—450 K.[14]

$$\begin{aligned} &2A = A_2, \\ &K = \frac{[A_2]}{[A]^2}. \end{aligned} \tag{16}$$

## Thermodynamic Properties

**Thermodynamic Properties under Ambient Pressure.** The thermodynamic properties are compared with MC[7] and the observed results[15—18] in Table 4, where the pressure ($P$) is fixed at 0.1 MPa. The calculated volume ($V$) deviates by 4—7%. The relative error in the potential energy ($E^e$) is 3—6%. The thermal expansion coefficient ($\alpha$,) isothermal compressibility ($\varkappa_T$) and excess heat capacity at constant pressure ($C_p^e$) are not very far from MC and the experimental

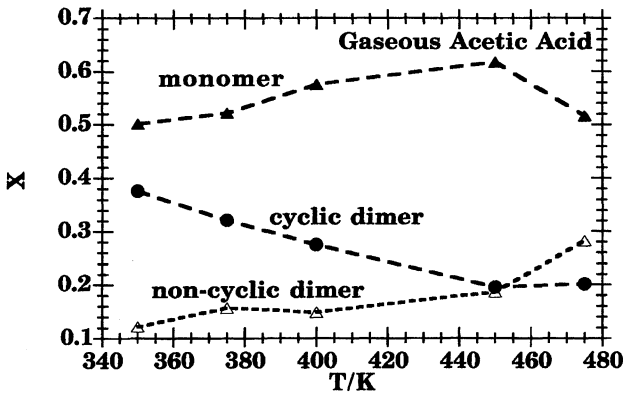


Fig. 16. The mole fraction $x$ of cyclic dimer, non-cyclic dimer, and monomer versus temperature $T$ plot in the gaseous phase. See the text for the method of analysis of the hydrogen bond.

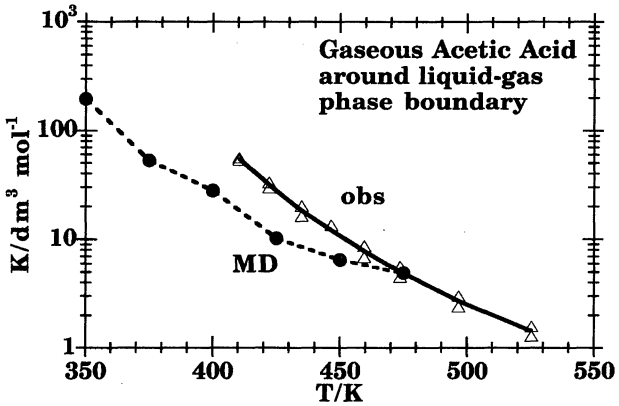


Fig. 17. The equilibrium constant $K$ of the chemical reaction of dimerization as a function of temperature $T$ in the gaseous phase. The calculated values are compared with the observed ones.[14]

values. Their temperature dependencies are qualitatively in accordance with the observations.

**Plot of the Thermodynamic Properties under Constant Pressure.** The excess entropy ($S^e$), and the excess heat capacity at constant pressure ($C_p^e$) are plotted against the reduced temperature ($T/T_c$) in Figs. 18 and 19. The reduced isothermal compressibility ($\varkappa_T^* P_c$) and the reduced thermal-expansion coefficient ($\alpha^* T_c$) are shown in Figs. 20 and 21, respectively. Anomalies around the critical point can be seen in these figures. The characteristics in the reduced isothermal compressibility ($\varkappa_T^* P_c$) and thermal-expansion coefficient ($\alpha^* T_c$) are similar to those in a Lennard–Jones (LJ) fluid[11] (not shown). Because of the dimerization in the gaseous phase, the excess heat capacity ($C_p^e$) of the gaseous state is not almost equal to zero, which is the case in the normal gas-like LJ model. The excess entropy ($S^e$) is discussed below.

**Comparison with Water.** As far as we know, there have been no extensive observations on fluid acetic acid

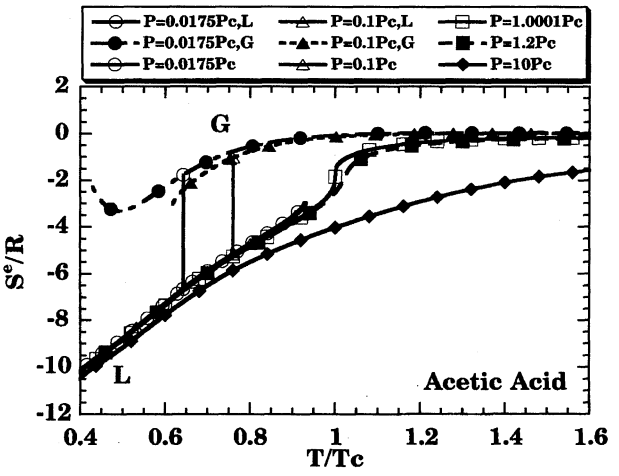


Fig. 18. The excess entropy of acetic acid $S^e$ versus reduced temperature $T/T_c$ plot under several pressures. The symbol L and G are attached to the liquid and gaseous phase, respectively.

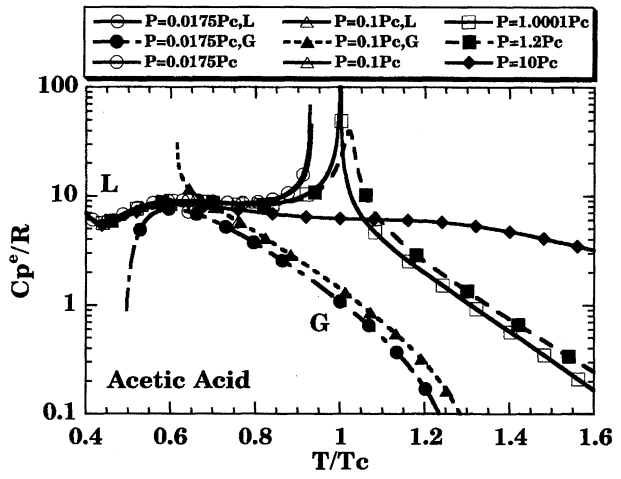


Fig. 19. The excess heat capacity at constant pressure of acetic acid $C_p^e$ versus reduced temperature $T/T_c$ plot under several pressures. The symbol L and G are attached to the liquid and gaseous phase, respectively.

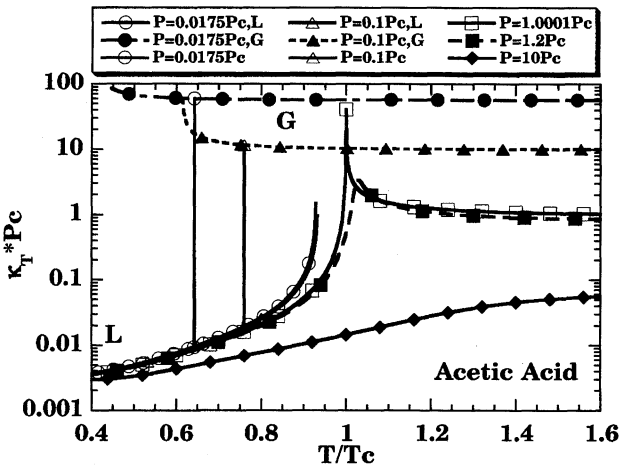


Fig. 20. The reduced isothermal compressibility of acetic acid $\varkappa_T^* P_c$ versus reduced temperature $T/T_c$ plot under several pressures. The symbol L and G are attached to the liquid and gaseous phase, respectively.

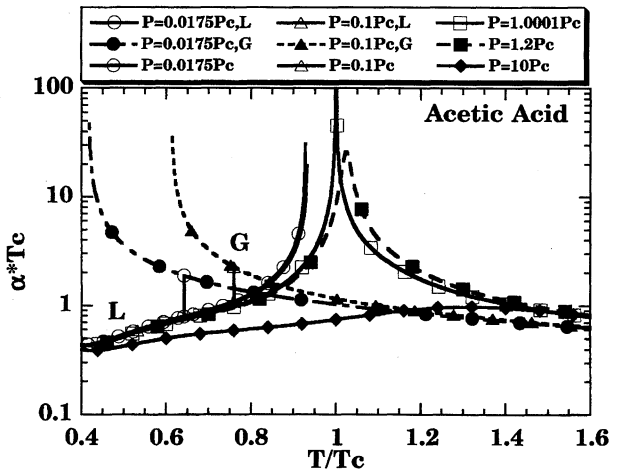


Fig. 21. The reduced thermal expansion coefficient of acetic acid $\alpha^* T_c$ versus reduced temperature $T/T_c$ plot at several pressures. The symbol L and G are attached to the liquid and gaseous phase, respectively.

over a wide rage of pressures and temperatures. For this reason, we are going to compare our calculated thermodynamics quantities with those of water, which is a well-known hydrogen-bonded system. Figure 22 gives the excess entropy ($S^e$), the excess heat capacity at constant pressure ($C_p^e$), the reduced isothermal compressibility ($\varkappa_T^* P_c$) and the reduced thermal expansion coefficient ($\alpha^* T_c$) of water.[19] These were calculated from the equation of state determined by the experimental results.[19]

The excess entropy ($S^e$) of acetic acid in the liquid phase is $-10\ R$ at low temperatures in Fig. 18. This is compared with the $-8\ R$ for water at the same reduced temperature ($T/T_c$=0.40). This was not expected. The density of liquid water under normal pressure is close to that of low-density ice. (The liquid density ($\rho_L$) is normalized by that of dense solid ($\rho_S$) in Table 5). It has large vacancies. For this reason, the liquid water has a low density compared to that of acetic acid. This difference in density is the reason for the unexpected relation in the excess entropy. The sharpness of the anisotropic interaction in Fig. 3 is another cause for the higher ordering in acetic acid. The effect of dimerization in the gaseous phase is not seen in the excess entropy of water.

The overall feature of the excess heat capacity at constant pressure ($C_p^e$) of water is similar to that of acetic acid. The acetic acid has larger heat capacities in the liquid phase compared to liquid water, if we compare those by the reduced temperature. The excess heat capacity at the constant pressure of liquid water has a minimum as a function of the temperature, as shown in the inset. This is a famous anomaly in liquid water. Although a similar anomaly is seen in Fig. 19 of liquid acetic acid, there is a possibility that this is spurious. This is a problem for fitting at low temperatures. The excess heat capacity at constant pressure of water in the gaseous phase is small because of no dimerization.

The reduced isothermal compressibility ($\varkappa_T^* P_c$) of liquid water is larger than that of acetic acid in the liquid phase. This is due to the low density of liquid water. That also has a minimum as a function of the temperature, as can be seen in Fig. 22. The compressibility of water is also larger than that of acetic acid in the gaseous phase. This results from the high density of acetic acid gas with dimerization.

The thermal-expansion coefficient ($\alpha^* T_c$) of liquid water under normal pressure has zero point at low temperature. Because of this effect, water has a smaller expansion coefficient than acetic acid in the liquid phase. In the other states, the general feature is similar in Figs. 21 and 22.

**Comparison of Excess Entropy with an LJ Fluid.** The excess entropy ($S^e$) of an LJ fluid is shown as a function of the reduced temperature in Fig. 23 at constant pressure. Note that the volume dependence of the entropy in the ideal gas is not the target of our discussion. The ideal gas term is subtracted in order to obtain the excess entropy. The excess entropy ($S^e$) in the normal liquid density has a value of around $-4R$ in the case of an LJ fluid. On the other hand, $S^e$ in an acetic acid liquid is $-10R$. This difference comes from the chains of the hydrogen bond in the acetic acid, as shown in Fig. 4. As for the gaseous phase of the LJ model, $S^e$ is almost zero.

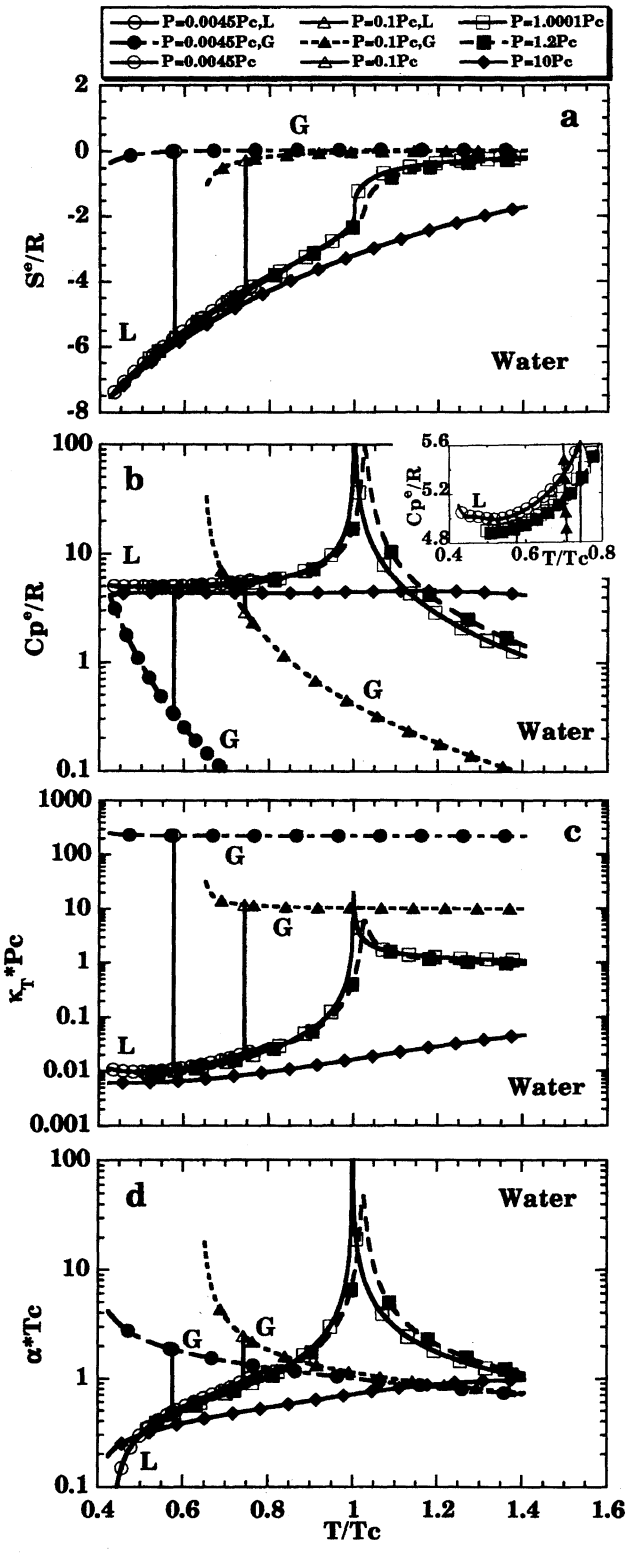


Fig. 22. The excess entropy $S^e$ (a), the excess heat capacity at constant pressure $C_p^e$ (b), the reduced isothermal compressibility $\varkappa_T^* P_c$ (c), and the reduced thermal expansion coefficient $\alpha^* T_c$ (d) of water[19] versus reduced temperature $T/T_c$ plot at several pressures. The symbol L and G are attached to the liquid and gaseous phase, respectively.

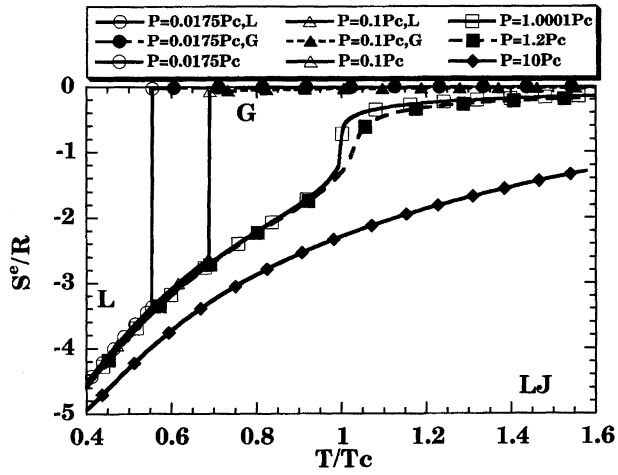


Fig. 23. The excess entropy $S^e$ of LJ fluid[11] versus reduced temperature $T/T_c$ plot under several pressures. The symbol L and G are attached to the liquid and gaseous phase, respectively.

Contrary to this, a value about $-1R$ can be seen in Fig. 18 as the excess entropy ($S^e$) in the gaseous phase of the acetic acid under low pressures. This is due to dimerization in the acetic acid gas at low temperatures.

The excess entropy ($S^e$) is as follows at the critical point:

$$\begin{aligned} &S^e/R \text{ (acetic acid)} = -1.8, \\ &S^e/R \text{ (water)} = -1.9, \text{ at the critical point,} \\ &S^e/R \text{ (LJ)} = -1.0. \end{aligned} \tag{17}$$

Although the difference of $S^e$ between acetic acid and water becomes small at the critical point, $S^e$(LJ) shows less ordering in an LJ fluid than in the hydrogen bonded systems (acetic acid and water).

**Quantitative Comparison of Liquid Acetic Acid with Water and an LJ Liquid.** The thermodynamic quantity ($Q$) of liquid acetic acid near to the triple point is compared with those of water and an LJ liquid in Table 5. In the last column, a ratio ($Q$ (acetic acid)/$Q$ (LJ)) is shown, where $Q$ (acetic acid) is the observed value when it is known. We can see that the reduced temperature ($T/T_c$), density ($\rho/\rho_c$) and pressure ($P/P_c$) of the state near to the triple point of acetic acid is close to those of the LJ system. The reduced thermal-expansion coefficient ($\alpha^* T_c$) of acetic acid around the triple point also has a value not far from that of an LJ liquid. The reduced isothermal compressibility ($\varkappa^* P_c$) of acetic acid is only 53% of that of the LJ case.

The large effects of the hydrogen bond appear in the excess heat capacity at constant volume ($C_v^e$) and pressure ($C_p^e$). Similar phenomena are found in the reduced excess internal energy ($E^e/RT_c$) and excess entropy ($S^e$). The excess entropy has already been discussed. The reduced excess internal energy means the reduced average potential energy. The ratio of this to that of the LJ system is 1.76. The values of the reduced excess internal energies of the discussed systems are almost the same as follows at the critical point:

Table 5. Thermodynamic Properties of Liquid Acetic Acid Near the Triple Point Compared with Water and LJ Liquid

| $Q$ | Acetic acid | | Water | LJ | $Q$ (acetic acid)/$Q$(LJ) |
|---|---|---|---|---|---|
| | EOS | Obsd[12,20] | EOS[19] Obsd[21] | EOS[11] | |
| $T/T_c$ | 0.424 | 0.4875 | 0.4234 | 0.4240 | 1.15 |
| $\rho/\rho_c$ | 3.34 | 3.004 | 3.110 | 2.573 | 1.17 |
| $P/P_c$ | 0.0175 | 0.0173 | 0.00453 | 0.01750 | 0.989 |
| $\alpha^* T_c$ | 0.443 | 0.64 | −0.0409 | 0.573 | 1.12 |
| $\varkappa_T^* P_c$ | 0.00388 | | 0.0112 | 0.00731 | 0.53 |
| $C_v^e/R$ | 4.08 | | 6.11 | 1.51 | 2.70 |
| $C_p^e/R$ | 5.81 | 7.09 | 5.11 | 3.48 | 2.04 |
| $E^e/RT_c$ | −9.38 | | −7.94 | −5.32 | 1.76 |
| $S^e/R$ | −9.80 | | −7.54 | −4.33 | 2.26 |
| $\rho_L/\rho_S$[a] | | 0.83 | 0.60 | 0.85 | 0.98 |

a) The quantities $\rho_L$ and $\rho_S$ are the density of liquid and that of the dense solid, respectively.

$$E^e/RT_c \text{ (acetic acid)} = -2.6,$$
$$E^e/RT_c \text{ (water)} = -3.1, \text{ at the critical point,} \quad (18)$$
$$E^e/RT_c \text{ (LJ)} = -2.6.$$

From this relation, it can be understood that the anisotropic potential well due to the hydrogen bond is deeper at low temperature in acetic acid than in a simple liquid with the same critical temperature ($T_c$). That well is averaged out to the value shown in Eq. 18 when the temperature increases and the density decreases to the critical point.

The liquid density is normalized by that of a dense solid in the last row. The ice VIII is used as a dense solid in the case of the water system. The normalized density ($\rho_L/\rho_S$) of acetic acid is almost the same with that of the LJ case. No significant effects of the hydrogen bond appear in the acetic acid liquid near to the triple point.

This work was supported in part by Grants-in-Aid for Scientific Research (Nos. 01540398, 02245209, and 03231211) from the Ministry of Education, Science and Culture. The authors thank the Computer Center of the Institute for Molecular Science for the use of computers. A part of the computation in this work was done using the facilities of the Super Computer Center, Institute for Solid State Physics, The University of Tokyo. The computation was also done at the Hosei University Computer Center and by CM-5 at College of Engineering, Hosei University.

## References

1) K. Yasuoka, M. Matsumoto, and Y. Kataoka, *J. Chem. Phys.*, **101**, 7904 (1994).
2) M. Matsumoto, K. Yasuoka, and Y. Kataoka, *J. Chem. Phys.*, **101**, 7912 (1994).
3) M. Faubel and Th. Jisters, *Nature*, **339**, 527 (1989).
4) M. Matsumoto and Y. Kataoka, *J. Chem. Phys.*, **88**, 3233 (1988).
5) M. Matsumoto and Y. Kataoka, *J. Chem. Phys.*, **90**, 2398 (1989).
6) M. Matsumoto, Y. Takaoka, and Y. Kataoka, *J. Chem. Phys.*, **98**, 1464 (1993), and references therein.
7) J. M. Briggs, T. B. Nguyen, and W. L. Jorgensen, *J. Phys. Chem.*, **95**, 3315 (1991).
8) M. P. Allen and D. J. Tildesley, "Computer Simulation of Liquids," Oxford Univ. Press, Oxford (1987).
9) F. H. Ree, *J. Chem. Phys.*, **73**, 5401 (1980).
10) Y. Kataoka, *J. Chem. Phys.*, **87**, 589 (1987).
11) J. J. Nicolas, K. E. Gubbins, W. B. Streett, and D. J. Tildesley, *Mol. Phys.*, **37**, 1429 (1979).
12) J. Timmermans, "Physico-Chemical Constants of Pure Organic Compounds," Elsevier, New York (1950), Vol. 1.
13) M. Fujita and H. Nishiumi, private communications. See H. Nishiumi, S. Kura, and T. Yokoyama, *Fluid Phase Equilib.*, **69**, 141 (1991).
14) E. Bich, A.-K.- Neumann, and E. Vogel, *Fluid Phase Equilib.*, **125**, 67 (1996).
15) J. L. Hales, H. A. Gundry, and J. H. Ellender, *J. Chem. Thermodyn.*, **15**, 211 (1983).
16) D. D. Wagman, W. H. Evans, V. B. Parker, R. H. Schumm, I. Halow, S. M. Bailey, K. L. Churney, and R. L. Nuttall, *J. Phys. Chem. Ref. Data, Suppl. 2*, **11**, 2 (1982).
17) J. Chao and B. J. Zwolinski, *J. Phys. Chem. Ref. Data*, **7**, 363 (1976).
18) J. W. Armitage and P. Gray, *Trans. Faraday Soc.*, **58**, 1746 (1962).
19) J. Kestin, J. V. Sengers, B. Kamgar-Parsi, and J. M. H. Levelt Sengers, *J. Phys. Chem. Ref. Data*, **13**, 175 (1984).
20) T. E. Daubert and R. P. Danner, "Physical and Thermodynamic Properties of Pure Chemicals: Data Compilation," Hemisphere Publishing Corporation, New York (1989).
21) D. Eisenberg and W. Kauzmann, "The Structure and Properties of Water," Oxford U. P., London (1969).